Environmental Science Nano

ROYAL SOCIETY OF CHEMISTRY

PAPER

View Article Online
View Journal | View Issue

Cite this: *Environ. Sci.: Nano*, 2021, **8**, 2336

Direct analysis of fulvic acids adsorbed onto capped gold nanoparticles by laser desorption ionization Fourier-transform ion cyclotron resonance mass spectrometry†

Konstantinos Giannopoulos,[a] Pietro Benettoni,[b] Timothy R. Holbrook,[a] Thorsten Reemtsma,[ac] Stephan Wagner ‡*[a] and Oliver J. Lechtenfeld *[a]

Natural organic matter (NOM) adsorption on nanoparticle (NP) surfaces in natural waters forms a corona that can alter NP properties and its environmental fate. Anthropogenic NPs are usually coated with an organic capping agent that may, in turn, influence the extent and molecular composition of the corona. Up-to-now, the molecular composition of the NOM corona can only be analyzed in controlled experiments due to a lack of appropriate direct surface analysis methods. Here, we introduce laser desorption ionization Fourier-transform ion cyclotron resonance mass spectrometry (LDI-FT-ICR-MS) to directly analyze Suwannee River Fulvic Acid (SRFA) after adsorption and sequential desorption on gold (Au) NPs capped with small molecules (citric acid (CA), tannic acid (TA), lipoic acid (LA)) and large polymers (polyvinylpyrrolidone (PVP), branched polyethylenimine (BPEI), methoxy polyethylene glycol sulfhydryl (m-PEG-SH)). LDI-FT-ICR-MS revealed differences in the molecular composition of the NP corona depending on the capping agents' chemistry. Positively charged BPEI efficiently adsorbed larger oxygen-rich aromatics whereas negatively charged CA and LA adsorbed oxygen-containing aromatics. The weak negative PVP adsorbed oxygen-containing aliphatics and non-charged m-PEG-SH small oxygen-depleted aliphatics, both with lower efficiency. However, TA preferentially adsorbed polyphenolic compounds from SRFA due to its similar chemistry. Further comparison of the Au-CA corona with the conventional indirect electrospray ionization (ESI)-FT-ICR-MS analysis largely confirmed the results of the new direct LDI analysis. Due to the higher sensitivity of the direct method, LDI-FT-ICR-MS can be applied to environmentally relevant NOM : NP ratios which was not possible before. LDI-FT-ICR-MS is a promising method to study the extent and molecular composition of NP coronas and suitable to better elucidate NP fate in the environment.

Received 16th December 2020,
Accepted 5th June 2021

DOI: 10.1039/d0en01253j

rsc.li/es-nano

Environmental significance

Nanoparticles (NPs) are widely used in different applications in our daily life and thus, do enter into the environment. Natural organic matter (NOM) attaches to the NP surface, forming a NP corona. The characteristics of this corona affect the fate and behaviour of NPs. In this study, laser desorption ionization Fourier-transform ion cyclotron resonance mass spectrometry (LDI-FT-ICR-MS) proved to be an appropriate method to directly characterize the molecular composition of the corona on NPs surfaces. It can be further used to investigate the relationship between the molecular composition of the adsorbed NOM molecules and NP fate and behavior. Such tools are key for predicting NP fate in the environment.

Introduction

After release into aquatic environments, nanoparticles (NPs) are exposed to dissolved natural organic matter (NOM), being a pool of diverse chemical compounds derived from exudates, leachates, and microbial decomposition of organisms.[1,2] These dissolved molecules may form a layer around the NP, and the term 'corona' was coined for this spontaneously assembled layer of organic molecules onto NP surfaces. NPs are often produced with a capping agent which modifies their interaction with NOM.[3,4] Yet, the corona itself

[a] *Department of Analytical Chemistry, Helmholtz Centre for Environmental Research – UFZ, Permoserstraße 15, 04318 Leipzig, Germany. E-mail: stephan.wagner@hof-university.de, oliver.lechtenfeld@ufz.de*
[b] *Department of Isotope Biogeochemistry, Helmholtz Centre for Environmental Research – UFZ, Permoserstraße 15, 04318 Leipzig, Germany*
[c] *Institute of Analytical Chemistry, University of Leipzig, Linnéstraße 3, 04103 Leipzig, Germany*

† Electronic supplementary information (ESI) available. See DOI: 10.1039/d0en01253j

‡ Current affiliation: Institute of Water- and Energy Management, University of Applied Sciences Hof, Alfons-Goppel-Platz 1, 95028 Hof, Germany.

plays a determining role in the behavior and fate of NPs.[2] It influences the adsorption of chemicals to the NP surface as well as aggregation, dissolution, and surface transformation of NPs.[5] For instance, it was demonstrated that aggregation of gold (Au) NPs was affected by the adsorption of NOM, which, in turn, was influenced by the engineered coating.[6,7] However, little is known about how the NP physicochemical properties such as size, charge, and surface functional groups influence the corona composition.[2] For example, the influence of the capping agent on the adsorption of NOM at environmentally relevant NOM : NP ratios (*i.e.* NOM : NP = 10^2–10^6)[6] has not yet been investigated in a systematic approach at the molecular level.

Adsorption of NOM on NPs can be detected indirectly, *e.g.* by changes in NP size, electrophoretic mobility, or their toxicity.[2] However, the chemical composition of the adsorbed material remains often unknown.[4] Spectroscopic methods provide direct evidence of the formation of a corona through changes in chemical functional groups.[8,9] They can also be used to study overcoating or replacement of the initial capping agents.[10,11] The preferential adsorption of different molecular weight fractions of NOM can additionally be investigated with chromatographic methods.[12,13] However, all these mentioned techniques lack information on the molecular composition of the corona. Therefore, techniques are needed which provide comprehensive details about the adsorbed molecules and their chemical characteristics to gain deeper insights into the constitution of the corona and its role for NP fate.

Ultrahigh-resolution mass spectrometry, such as Fourier-transform ion cyclotron resonance mass spectrometry (FT-ICR-MS), provides sufficient mass resolution (>200 000 $m/\Delta m$) and mass accuracy (mass error < 1 ppm) to resolve molecular-ion peaks in complex NOM mixtures and to reliably assign molecular formulas.[14,15] FT-ICR-MS with electrospray ionization (ESI) has been used to analyze compositional differences in NOM solutions before and after contact with mineral surfaces.[16–23] Using such an indirect approach, the molecular composition of a corona formed by NOM on silver (Ag) NPs coated with citrate was previously described.[24] However, the limited sensitivity of the indirect detection method usually requires low NOM : NP ratios, which may affect the selectivity of the NOM sorption as compared to natural systems.

In contrast to ESI, where a liquid sample is introduced into the mass spectrometer to create charged droplets from which the ions are ejected,[25] laser desorption ionization (LDI) analyzes solid samples *via* laser irradiation. Thus, liquids or suspensions need to be first deposited and dried on a dedicated target, usually a conductive glass slide or metal plate. Since most metal NPs absorb the laser energy at commonly utilized laser wavelengths (*e.g.* Nd:YAG with 355 nm) the coating of the NPs can be ionized.[26] Thus, LDI-MS allows the direct analysis of molecules on NP surfaces from dried NP suspensions. For instance, LDI-time-of-flight-MS can be used to identify the capping agent and the NP core material and also changes in the capping agent composition after interaction with organic solutes.[27] Based on these findings, it was assumed that ultrahigh-resolution LDI-FT-ICR-MS would provide the most detailed information on the molecular composition of the corona formed from NOM on NPs. Such a direct analysis of the corona composition has notable advantages over the indirect approach: (a) it is suitable for NPs collected from the environment where the initial solution prior adsorption is not available, (b) it allows studying processes such as overcoating and replacement of the capping agent, (c) it can be used to conduct mechanistic studies at environmental meaningful NOM : NP ratios and (d) no extraction step is needed to extract the adsorbed molecules from the NP surfaces or the dissolved molecules in the supernatant. The latter is especially important when working in buffered systems, as the sample matrix usually precludes direct ESI-MS measurements of dissolved NOM.

Here, we introduce LDI-FT-ICR-MS as a technique for the direct molecular analysis of coronas formed on the surface of Au NPs. Small organic molecules, as well as large synthetic polymers with different surface charge, size, functional groups, and binding mechanism to the core were selected as representative capping agents. Au NPs were chosen as a model NP due to their chemical stability, known surface chemistry, and the great variety in available surface functionalizations.[2,28] Suwannee River Fulvic Acid (SRFA) was used in 100-fold excess over NPs to mimic environmental relevant ratios. SRFA was selected as terrestrial originated NOM because it is well-characterized and highly water-soluble, representing the major fraction of aquatic dissolved NOM. The developed LDI-FT-ICR-MS method can be used for such high NOM : NP ratios and provides complementary information to the conventional indirect analysis using ESI-FT-ICR-MS. We applied this method to investigate the extent of which the capping agent influences the adsorption of NOM to NPs.

Materials and methods

Chemicals

Au NPs (56.8 mg L^{-1}, 60 nm) capped with citric acid (CA) were purchased from BBI solutions (Cardiff, UK). Au NPs (50 mg L^{-1}, NanoXact, 60 nm) capped with lipoic acid (LA), tannic acid (TA), polyvinylpyrrolidone (40 kDa PVP), branched polyethylenimine (25 kDa BPEI), methoxy polyethylene glycol sulfhydryl (5 kDa m-PEG-SH) were purchased from nanoComposix (Prague, Czech Republic). Suwannee River Fulvic Acid (SRFA) standard II was purchased from the International Humic Substances Society (St. Paul, USA). SRFA stock solutions with two different concentrations of 5.6 g SRFA L^{-1} and 5.0 g SRFA L^{-1} were prepared in MilliQ water (MilliQ Integral 5, Merck, Darmstadt, Germany) to compensate for the differing NP concentrations in the standards. LC-MS grade methanol (MeOH) was purchased from Biosolve (Valkenswaard, Netherlands).

Adsorption experiments

1 mL of SRFA solution was mixed with 1 mL of Au NPs suspended in water in a 2 mL Eppendorf Safe-Lock tube to obtain a concentration ratio [SRFA : Au NPs] of ~100 : 1 (m/m). The suspension was shaken for 2 h at 50 rpm (360° Multifunction Tube Rotator, PTR-35, VWR International, LLC). Zeta potential of the NP stock suspension and the suspension after mixing with SRFA was determined with a Zetasizer Ultra (Malvern Panalytical, Malvern, UK). The suspension was centrifuged at 15 000 rpm for 10 min at 4 °C using a bench-top centrifuge (Eppendorf 5424 R, Eppendorf AG, Wesseling-Berzdorf, Germany). The supernatant (referred to as "solution after adsorption") was removed using a syringe. The remaining NP suspension (~20 μL: "NPs after adsorption") was homogenized by ultra-sonication with a VialTweeter (UP200St, Hielscher Ultrasound Technology, Teltow, Germany) and contained a 50-fold higher NP concentration than the initial suspension. This 1st centrifugation step removed excess SRFA solution after adsorption onto the NPs, yet retains the initial SRFA concentration in the concentrated NP suspension (*i.e.* 2.5 or 2.8 g SRFA L^{-1} depending on the used SRFA solution). Due to the 100-fold excess of SRFA in this adsorption step, no detectable change in the SRFA concentration or composition in solution after adsorption is expected. The pH value of the highly concentrated SRFA solution (Table S2†) was not adjusted or buffered to allow for a direct ESI measurement of the supernatant after adsorption (*i.e.* without further extraction step).

Desorption experiments

The concentrated NP suspension after the adsorption step was diluted with 2 mL of MilliQ water and shaken for 30 min at 50 rpm. After subsequent centrifugation, the supernatant (now referred to as "solution after 1st desorption") was removed, and the remaining NP suspension (now referred to as "NPs after 1st desorption") was treated with the VialTweeter. This procedure was again repeated to obtain the final NP suspension ("NPs after 2nd desorption") and supernatant ("solution after 2nd desorption"). Each dilution-centrifugation step represents a 1 : 100 dilution of the SRFA solution which was still present in the concentrated NP suspensions (*i.e.* NPs after 1st desorption contained ~25 or ~28 mg SRFA L^{-1}; NPs after 2nd desorption contained ~250 or ~280 μg SRFA L^{-1}; depending on the used SRFA solution). In contrast, the NP concentration in each concentrated suspension (*i.e.* after adsorption and after two desorption processes) remains constant (*i.e.* ~2.5 or ~2.8 g NPs L^{-1}; depending on the used NP suspension) assuming no loss of NPs during sample handling. The pH of the suspension was not further adjusted and increased from 2.6 after adsorption to 5.1 after two desorption steps due to the dilution with MilliQ water (Table S2†). With respect to the adsorbed SFRA molecules on the NPs, the 1st and 2nd desorption represent new sorption–desorption equilibria with the potential for desorption of specific SRFA molecules from the NPs, partly also due to the increase in pH. This desorption from the NPs is expected to result in detectable changes in the composition of SRFA in the solutions after the 1st and 2nd dilution-centrifugation step. A scheme for the adsorption and desorption experiments is shown for the CA capped Au NPs (abbreviated as Au-CA) in the ESI† in Fig. S1.

Preparation of Au-CA – SRFA reference sample for LDI

2 mL of Au-CA suspension was bath sonicated with 35 kHz for 3 min (Bandelin Sonorex Digitec DT 1028 CH, Berlin, Germany), vortexed for 1 min at a speed of 2850 rpm (Digital Vortex-Genie 2, Scientific Industries, Inc., New York, USA), centrifuged, the supernatant removed, and the remaining NP suspension was treated with the VialTweeter as described above. From this concentrated NP suspension, 10 μL were mixed with 10 μL SRFA stock solution (5.6 g L^{-1}) and used as a reference sample for LDI analysis ("Au-CA – SRFA reference"). The concentrated NP suspension used for LDI analysis still contains dissolved SRFA (see above) which may co-ionize together with the molecules which form the corona in suspension. Hence, this reference sample represents a LDI measurement where the NPs are only used to support desorption and ionization of SRFA, whereby the SRFA is detected as it is present in solution since no sample treatment was performed. By comparing the Au-CA – SRFA reference sample with the Au-CA after adsorption, changes in the relative abundance of specific molecules then indicate selective adsorption on the NPs. Moreover, by comparing this reference sample with the differently capped Au NPs after the 2nd desorption, the general influence of the capping agent on the adsorbed molecule characteristics is obtained. This reference sample was prepared in triplicates to assess method and instrumental variability on signal detection and mass peak intensity. Fig. S2† illustrates the preparation procedure of this Au-CA – SRFA reference sample.

FT-ICR-MS measurements

A dual source ESI/MALDI-FT-ICR mass spectrometer equipped with a dynamically harmonized analyzer cell (solariX XR, Bruker Daltonics Inc., Billerica, MA, USA) and a 12 T refrigerated actively shielded superconducting magnet (Bruker Biospin, Wissembourg, France) instrument was used. The instrument was operated in broadband mode (mass range 150–1000 m/z) with a 4 MW time domain (mass resolution at m/z 400: ~483 000) and initially calibrated using SRFA.

For LDI experiments, the concentrated NP suspensions from each treatment step were prepared by depositing 3 × 0.5 μL on a Stainless Steel target (384 MTP ground steel, Bruker Daltonics, Bremen, Germany). Samples were measured in negative ionization mode. MALDI source (Smartbeam II) parameters were as follows: for each spectrum, 10–20 laser shots with spot size setting "ultra" and 10% laser power were used. A total of 256 spectra were randomly acquired on the target using selective accumulation, resulting in comparable total ion counts (TIC) between spectra (8.3–24.2 × 10^{10}).

Further spectra details of each sample for the LDI measurements are shown in Table S1.†

For ESI measurements, the SRFA stock solution (also referred to as "SRFA reference") and the solution of Au-CA after adsorption were diluted to ~28 mg L^{-1}. The solutions of Au-CA after 1st desorption (~28 mg L^{-1}) and after 2nd desorption (~280 μg l^{-1}) were not diluted but directly measured. All these solutions were mixed 1 : 1 (v/v) with MeOH before ESI measurement. The SRFA reference was analyzed three times to assess instrumental variability on signal detection and intensity. Samples were measured in negative ionization mode (capillary voltage: 4.3 kV) with an autosampler (infusion rate: 10 μL min^{-1}). For each spectrum, 256 scans were co-added with 10–20 ms ion accumulation time (IAT). However, a significant higher IAT was used for the solutions after the 2nd desorption to compensate for its lower carbon concentration, resulting in comparable TIC between spectra (10.1–16.0 × 10^{10}). Further spectra details of each sample for the ESI measurements are shown in Table S1.†

Mass spectra were internally recalibrated with a list of 188 masses (between 247–643.1 *m*/*z*) commonly found in SRFA, and calibrant masses with errors > |0.2| ppm were removed. Depending on the total intensity of LDI spectra, between 19 and 188 calibrants were used and the resulting mass accuracy after linear calibration was better than 0.1 ppm (n = 22). For ESI spectra, respective values were: 155–181 calibrants and <0.06 ppm (n = 6). Peaks were considered if the signal-to-noise (S/N) ratio was greater than 4. Raw spectra were processed with Compass DataAnalysis 5.0 (Bruker Daltonics Inc., Billerica, MA, USA).

FT-ICR-MS data processing

Molecular formulas (MFs) were assigned to peaks in the range 150–1000 *m*/*z* allowing for elemental compositions $C_{1-80}H_{1-198}N_{0-2}O_{0-40}S_{0-1}$ with an error range of ±0.4 ppm according to Lechtenfeld *et al.*[29] The highest NOM peak was manually identified in each spectrum and set as 100% signal intensity whereby all peaks with a higher signal intensity (*e.g.* Au-cluster ions) were excluded. For LDI mass spectra, the following compositional ranges were applied: 0 ≤ H/C ≤ 3, 0 ≤ O/C ≤ 1.2, 0 ≤ N/C ≤ 1.5, 0 ≤ DBE ≤ 50 (double bond equivalent, DBE = 1 + 0.5·(2C − H + N)), −10 ≤ DBE-O ≤ 20, and element probability rules proposed by Kind and Fiehn.[30] For ESI mass spectra H/C was limited to 0.3–3, DBE to 0–25, and DBE-O to −10–10 as proposed by Koch *et al.* and Herzsprung *et al.* for ESI measurements of SRFA.[31,32] Isotopologue formulas (^{13}C, ^{34}S) were used for quality control but removed from the final data set as they represent duplicate chemical information. MFs from solvent blanks (MilliQ water + MeOH) were removed from the ESI mass lists. Bulk sample molecular descriptors of peak intensity weighted average values were calculated for H/C, O/C, N/C, S/C, N/S, DBE, DBE-O, and AI (aromaticity index:[33] (1 + C − O − S − 0.5·(H + N))/(C − O − S − N)), whereas for the molecular weight (M_w) the simple mean was used. It is worth mentioning that these molecular descriptors are not influenced by fragments derived from the capping agents since they were either excluded by the formula assignment rules (limited by N_2S_1 and mass range) or could not be detected as molecular formulas within the data set.

Data visualization

The assigned MFs and the corresponding ratios of H/C and O/C were used to reconstruct mass spectra and to plot van Krevelen diagrams (VKD),[34] respectively. The VKD displays relative signal intensities (RI) normalized to the highest intensity of the assigned MFs and expressed as a color scale where the H/C and O/C ratio of each MF are plotted against each other. A diagram of H/C *vs.* molecular mass is used for complementary information on molecular mass. For the ease of comparison between two samples, the differences in relative signal intensities of common assigned MFs can be calculated as $\Delta RI = RI_{sample\_A}/(RI_{sample\_A} + RI_{sample\_B})$[35] and shown in a comparison VKD (cVKD) and comparison H/C *vs.* molecular mass diagrams. To compare multiple samples, their bulk molecular H/C *vs.* O/C values are shown in an aggregated VKD (aVKD).

Results and discussion

Direct corona characterization on Au-CA by LDI-FT-ICR-MS

In order to investigate the applicability of LDI for the direct analysis of the corona formed on NPs, CA capped Au NPs were mixed with SRFA in an environmental relevant ratio. After the initial adsorption step, two desorption steps were performed to investigate changes in the NP corona due to differently bound SRFA molecules. This experimental setup was performed to mimic NOM interactions with NPs after their release into the aquatic environment. After each of these three treatment steps, the NPs were measured by LDI-FT-ICR-MS. The extent of the corona formation is inferred from the sum of SRFA signal intensities in the reconstructed spectra (TAI, total assigned intensity) and the number of assigned MFs. The chemical composition of the corona is discussed based on the molecular descriptors calculated from the MFs.

In each of the LDI-FT-ICR-MS raw spectra, a characteristic NOM pattern was present indicating adsorption of SRFA (Fig. S3†). For Au-CA, 6432 MFs were detected after adsorption (TAI: 1.1 × 10^{11}), 5996 MFs (7.8 × 10^{10}) after 1st desorption, and 4171 MFs (3.5 × 10^{10}) after 2nd desorption, respectively (Table S1†). The decrease in TAIs and number of MFs indicates a loss of adsorbed molecules to the solution in each desorption step. Molecules detected after the adsorption step had a higher relative abundance at lower O/C, lower H/C ratios, and lower molecular mass as compared to the Au-CA – SRFA reference sample (Fig. S4†). This indicates that Au-CA NPs selectively adsorbed smaller unsaturated and oxygen-depleted molecules. Predominantly low O/C, low H/C, and low molecular mass MFs were detected in the corona of NPs

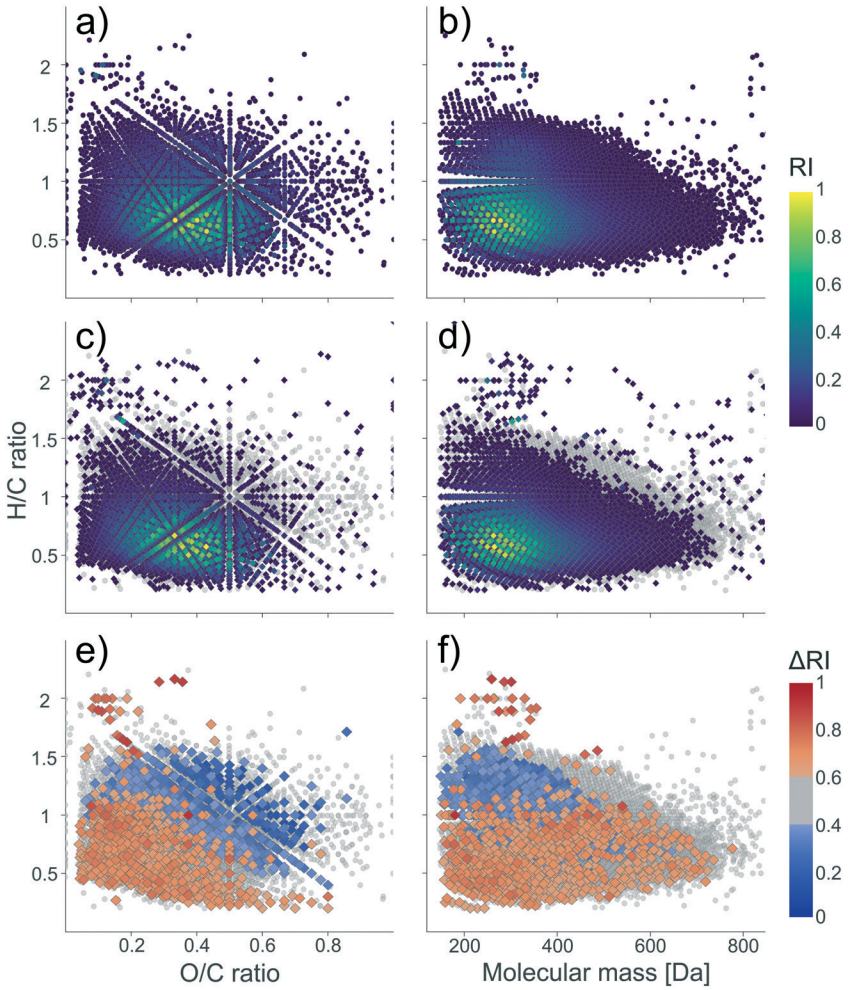

Fig. 1 The VKDs (a and c) and H/C *vs.* molecular mass diagrams (b and d) of molecular formulas detected by LDI-FT-ICR-MS measurements of Au-CA after adsorption (a and b) and Au-CA after 2nd desorption (c and d). The relative intensity (RI) of the corresponding mass peaks is displayed as color scale, and the formulas from Au-CA after adsorption are shown in c) and d) as reference in grey. In e) and f) the cVKD and comparison H/C *vs.* molecular mass diagram, respectively for Au-CA after 2nd desorption *vs.* Au-CA after adsorption is displayed. The ΔRI values calculated from relative peak intensities are shown as color scale whereby red colors ($0.6 \leq \Delta RI \leq 1$) represent formulas more abundant in Au-CA after 2nd desorption, blue colors ($0 \leq \Delta RI \leq 0.4$) represent formulas more abundant in Au-CA after adsorption, and here, the grey color indicates similar relative intensities ($0.4 \leq \Delta RI \leq 0.6$) for the common assigned MFs in both samples.

after 2nd desorption, which represents strongly bound molecules (Fig. 1).

Additional molecular descriptors for the corona on Au-CA are summarized in Table 1. After two subsequent desorption steps, the remaining molecules had a lower M_w, a higher ratio of N/C and S/C, a high number of DBE, DBE-O, and AI. These results indicate that in each desorption step, larger molecules with more aliphatic and oxygen-rich character were preferentially released from the surface. In contrast, aromatic and condensed aromatic molecules with a minor contribution of oxygen represent the strongly bound corona (Fig. 1). While some of these pronounced chemical properties are related to the ionization method and selected NOM sample, the direct comparison of the different NP suspensions revealed distinct molecular-level changes of the NP corona upon altered sorption–desorption equilibria. Moreover, the possible ionization of SRFA molecules in solution has only a minor influence on the detected NP corona composition. This is corroborated by the fact that the Au-CA – SRFA reference sample displays a substantially different molecular composition as compared to the Au-CA after adsorption, although both have nominally the same NP and SRFA concentrations. This comparison indicated that it is possible to detect NP corona composition even at high NOM : NP ratios. Overall, the LDI-FT-ICR-MS method has sufficient sensitivity to directly analyze the NP corona at low and high NOM : NP ratios and its compositional change as a result of the desorption processes under the applied analytical conditions.

The preferential and strong adsorption of aromatics and condensed aromatics onto the Au surface can be explained by the formation of π bonds. This is in agreement with the proposed regium–π bonds that are attractive noncovalent forces between aromatics and Au.[36–38] The high proportion of S in the adsorbed molecules can be attributed to the

Table 1 Molecular descriptors for the complete corona characterization of Au-CA derived from the LDI- and ESI-FT-ICR-MS measurements. The LDI measurement error (4.2%) was calculated from triplicate sample preparation of the Au-CA – SRFA reference sample and was used for all LDI measurements. For ESI, the measurement error (0.4%) was calculated from triplicate sample preparation of the SRFA reference sample and was used for all ESI measurements

	Sample name	M_w [Da]	O/C	H/C	N/C [$\times 10^3$]	S/C [$\times 10^3$]	N/S [$\times 10^3$]	DBE	DBE-O	AI
LDI-FT-ICR-MS	Au-CA – SRFA reference sample	458 ± 6	0.40 ± 0.01	0.83 ± 0.02	6.07 ± 0.13	0.98 ± 0.10	6.24 ± 0.74	12.80 ± 0.34	4.95 ± 0.37	0.39 ± 0.02
	Au-CA after adsorption	446 ± 19	0.37 ± 0.02	0.78 ± 0.03	6.04 ± 0.25	0.81 ± 0.03	7.48 ± 0.31	13.33 ± 0.56	6.09 ± 0.26	0.45 ± 0.02
	Au-CA after 1st desorption	440 ± 18	0.34 ± 0.01	0.71 ± 0.03	7.55 ± 0.32	1.43 ± 0.06	5.27 ± 0.22	14.69 ± 0.62	7.69 ± 0.32	0.54 ± 0.02
	Au-CA after 2nd desorption	413 ± 17	0.33 ± 0.01	0.70 ± 0.03	8.06 ± 0.34	1.97 ± 0.08	4.09 ± 0.17	14.29 ± 0.60	7.76 ± 0.33	0.55 ± 0.02
ESI-FT-ICR-MS	SRFA reference sample	385 ± 1	0.43 ± 0.00	1.11 ± 0.00	2.60 ± 0.12	0.94 ± 0.08	2.78 ± 0.35	8.90 ± 0.00	1.42 ± 0.01	0.17 ± 0.00
	Solution after adsorption	387 ± 2	0.43 ± 0.00	1.11 ± 0.00	2.75 ± 0.01	0.91 ± 0.00	3.01 ± 0.01	8.92 ± 0.04	1.37 ± 0.01	0.17 ± 0.00
	Solution after 1st desorption	413 ± 2	0.46 ± 0.00	1.10 ± 0.00	2.89 ± 0.01	0.39 ± 0.00	7.37 ± 0.03	9.19 ± 0.04	0.94 ± 0.00	0.14 ± 0.00
	Solution after 2nd desorption	365 ± 1	0.40 ± 0.00	1.21 ± 0.00	7.38 ± 0.03	3.41 ± 0.01	2.16 ± 0.01	8.20 ± 0.03	1.19 ± 0.00	0.15 ± 0.00

formation of Au–S bonds, which have a high binding energy of 40 kcal mol^{-1}.[39] Regarding N, the adsorption of electron-rich amines onto Au was also reported.[40] However, in comparison to thiols, amines have lower binding energies to Au surfaces.[40,41] This was also confirmed by the decreasing N/S ratio indicating the preferential desorption of N-containing compared to S-containing molecules (Table 1).

The interaction between Au-CA with NOM has already been reported in the literature. However, there is contradictory evidence related to the fate of the initial capping agent, which in the case of CA, is weak electrostatically bound and both, overcoating[10,11] and replacement[42,43] were discussed. Nevertheless, LDI-FT-ICR-MS results indicated that CA was replaced by SRFA molecules because, after the two desorption steps, the molecular ion signal of CA could no longer be detected (Fig. S5†). Notably, also the NP core material was confirmed by the presence of the Au-cluster ions in all analyzed samples (Fig. S3†).

Indirect corona characterization of Au-CA by ESI-FT-ICR-MS

For comparison with the conventional indirect corona determination, ESI-FT-ICR-MS measurements were performed with the SRFA reference sample, as well as the solutions after adsorption and the subsequent desorption steps. The use of ESI is not only a different ionization method as compared to LDI but also a different analytical approach since the initial SRFA solution is always needed to compare with the solutions of each treatment step (Fig. 2). Expectedly, using a NOM : NP ratio of 100 : 1, the compositional changes of the SRFA solution due to adsorption on the Au-CA were too small to be detected by ESI-FT-ICR-MS (Fig. 2a and b). However, the solutions after desorption revealed distinct molecular information on the desorbed molecules. SRFA molecules with high O/C, average H/C and high molecular masses were enriched in the solution after 1st desorption as compared to the solution after adsorption (Fig. 2c and d), suggesting that large, oxygen-rich molecules were only weakly bound to Au-CA. On the contrary, molecules with low O/C, high H/C, and low molecular masses preferentially desorbed during the 2nd desorption step (Fig. 2e and f). This indicates that more strongly bound molecules were small oxygen-deficient aliphatics. However, no information on the actual corona composition could be obtained with ESI-FT-ICR-MS. The VKDs of each solution and the SRFA reference sample, as well as the ESI-FT-ICR-MS raw spectra, are depicted in Fig. S6 and S7,† respectively.

Molecular descriptors of the desorbed SRFA are presented in Table 1: molecules present in the solution after 1st desorption had higher M_w, were more aromatic (low H/C and high DBE) with high oxygen content (high O/C and low DBE-O), and had a lower S/C ratio, as compared to the SRFA reference. Based on this information on the desorbed molecules, it can be inferred that the corona (after 1st

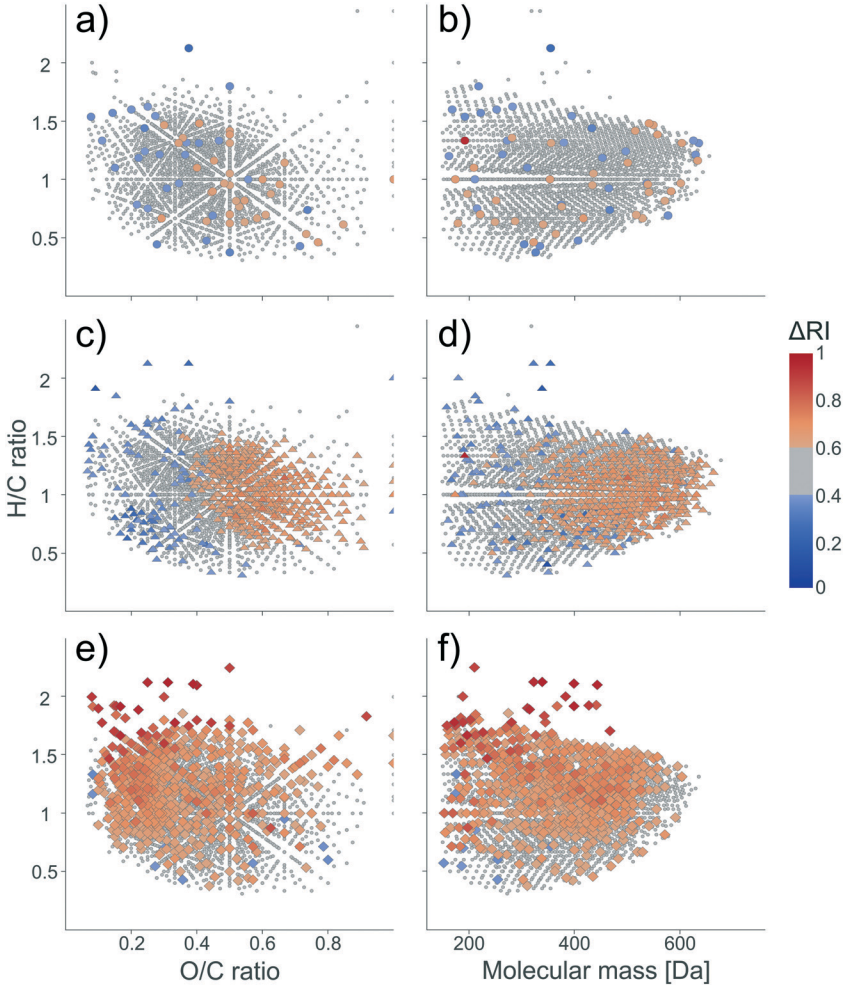

Fig. 2 The cVKDs (a, c, and e) and comparison H/C *vs.* molecular mass diagrams (b, d, and f) of molecular formulas detected by ESI-FT-ICR-MS measurements for the solution after adsorption (a and b), solution after 1st desorption (c and d), and solution after 2nd desorption (e and f) each *vs.* SRFA reference sample. The ΔRI values calculated from relative peak intensities are shown as color scale. Red colors ($0.6 \leq \Delta RI \leq 1$) represent formulas more abundant in the adsorption and desorption solutions, whereas blue colors ($0 \leq \Delta RI \leq 0.4$) represent formulas more abundant in the SRFA reference sample. Grey color indicates similar relative intensities ($0.4 \leq \Delta RI \leq 0.6$) for the common assigned MFs in both samples.

desorption) consisted of low M_w molecules with high saturation (high H/C and low DBE), low oxygen content (low O/C), and a high fraction of sulfur. The direct corona analysis (Au-CA after adsorption, Table 1) mirrored this general trend. However, the absolute values of molecular descriptors are dependent on the ionization method used and need to be considered independently.

The molecules detected in the solution after 2nd desorption were smaller (lower M_w), had a more aliphatic character (higher H/C and lower DBE) with a lower oxygen content (lower O/C), and a higher S/C ratio as compared to the solution after 1st desorption, indicating a shift in the chemical character of the desorbed molecules. In addition, a substantial increase of the N/C ratio revealed the detachment of N-containing molecules that preferentially desorbed as compared to O-containing molecules. In the solution after 2nd desorption (if compared to the solution after 1st desorption), the lower N/S ratio confirms the results obtained from the direct corona analysis that the N-containing molecules were loosely bound compared to S-containing molecules. It should be noted that only the combination of the molecules detected in the 1st and 2nd desorption solution may be used to approximate the initial corona composition. When using realistic NOM : NP ratios, the second desorption step is highly recommended in order to accurately characterize the initial corona composition with the indirect ESI method. In contrast, LDI-FT-ICR-MS revealed the chemical composition of the corona by the direct analysis of the NPs without the need of carrying out additional desorption steps for its confirmation. Nevertheless, the results from the indirect ESI-FT-ICR-MS analysis of the corona composition largely confirmed the direct LDI-FT-ICR-MS analysis. The comparison between ESI and LDI spectra for each adsorption and desorption step is shown in Fig. S8.†

The corona of Ag-CA NPs and two different NOM types have been previously investigated with ESI-FT-ICR-MS, indicating that the formed coronas varied with the NOM composition.[24] Our results further indicated that the

depiction of the molecular composition of the corona may vary with the number of adsorption and desorption steps (and presumably also NOM : NP concentration ratios and equilibrium times). Taken together, this suggests that NP–NOM interactions are very complex, and the resulting corona may differ depending on NP core and NOM composition and experimental setup. Thus, a comparison across different studies remains difficult as long as no standardized protocol is available that considers same or similar materials, experimental conditions, formula assignment, and data processing routines for the non-targeted ultrahigh-resolution MS data sets. Regarding NOM, due to the compositional variability of different NOM types, we recommend to always include SRFA in experimental setups to ease comparability and comprehensiveness of results across labs and NP–NOM interaction studies. Although unbuffered SRFA solutions deviate from natural systems in terms of pH and ionic strength, its use is advantageous for methodological comparisons, since the supernatant can be analyzed *via* ESI-MS without further extraction.

Influence of the capping agent on the corona composition

To further investigate the influence of capping agents on the corona formation on Au NPs, similar experiments were performed with five other capping agents, covering different kinds of interactions of the capping agent with the Au NPs and also allowing for different interactions of the capping agents with the SRFA solution. These capping agents can be categorized as small molecules TA and LA as well as large polymers PVP, BPEI, and m-PEG-SH varying in functional groups and surface charges (Table S2†). In all cases, initial mixing with SRFA solution lowered the zeta potential and decreased the pH of the Au NPs reflecting the (excess) SRFA (Table S2†). All NP suspensions were analyzed with LDI-FT-ICR-MS, and a complete overview of the data is shown in Table S3,† whereas the raw spectra for the five additional NP-capping agent combinations are shown in Fig. S9–S13.† All reconstructed mass spectra of the 2nd desorption are displayed in Fig. 3a. The characteristic NOM pattern was clearly visible from LDI-FT-ICR-MS even for the 2nd desorption revealing adsorption of SRFA on all differently capped Au NPs. The increase in pH due to dilution with MilliQ may have favored desorption of SRFA molecules. However, the corona composition observed by the LDI analysis represents the stable bound SRFA molecules at the respective pH. Differences in type and intensities of molecular formulas reflect the preferential adsorption of NOM molecules depending on the capping agents.

The number of assigned MFs after adsorption varied between capping agents and markedly decreased in all cases after each step to 28–75% after the 2nd desorption (Fig. 3b). BPEI, CA, and LA still showed the largest number of detected MFs with 4740, 4171, and 3934, respectively (decrease to 63–75%) which is in agreement with their higher TAIs (Fig. 3a). In contrast, PVP, m-PEG-SH, and TA had the lowest number of detected MFs with 2923, 1806, and 1809, respectively (decrease to 28–56%) which was also mirrored in the TAIs. In addition to the different extent of adsorption, also the chemical composition of adsorbed SRFA molecules revealed clear differences between capping agents.

The aggregated molecular descriptors after two desorption steps are shown in Fig. 3c–i. A trend of the SRFA coronas depending on the capping agent was visible in the order BPEI, CA/LA, PVP, and m-PEG-SH for the molecular descriptors H/C, O/C, M_w, DBE, and DBE-O whereby TA was a notable exception (see below). This trend was also visible for the corona extent represented by the TAIs and MFs (Fig. 3a and b). Overall, positively charged capping agents (BPEI) attracted many, large-sized, oxygen-rich, and aromatic molecules from SRFA, negatively charged capping agents of low molecular weight (CA, LA) attracted many, but on average medium-sized, medium oxygen-containing aromatics while the large and weak negatively charged (PVP) attracted aliphatics that are few, small-sized, and medium oxygen-containing. Finally, the large and neutrally charged capping agents (m-PEG-SH) attracted only few aliphatic, small-sized, and oxygen-depleted molecules.

However, comparing with the Au-CA – SRFA reference sample, the molecules adsorbed onto the NPs had, in general, a lower M_w, high unsaturation, and were poor in O but enriched in N and S (Fig. 3c–i). Especially the enrichment of S in all coronas may indicate that the NP core itself largely influences the adsorption behavior of NOM due to the high binding energy of Au–S bonds.[39] On top of that, the selective adsorption of NOM molecules onto NPs can be further explained by the functional groups of the capping agents that, in turn, determine the surface charge.

The methoxy end group of Au-(m-PEG-SH) displayed a neutral charge towards the solution and allowed only weak interaction with the mostly negatively charged oxygen-rich and aromatic compounds in SRFA. The oxyethylene groups allow hydrogen-bonding or attractive van der Waals forces[44] and promoted the attraction of molecules with a more aliphatic character and with low oxygen content as indicated by the highest H/C, lowest O/C, DBE, and low DBE-O values (Fig. 3c, e and f). PVP can also perform hydrogen-bonding[45] as well as van der Waals forces[46] with SRFA molecules and led to a similar adsorption behavior of attracting aliphatics as Au-(m-PEG-SH) (Fig. 3c, e and f). In both cases, the large molecular weight appears to prevent an extensive and strong corona formation as well as the attraction of larger molecules (Fig. 3a, b and d). However, the ability of the cyclic amide in PVP to form hydrogen-bonding may explain the adsorption of molecules with a higher number of oxygen (Fig. 3c) and the strong adsorption of nitrogen-containing compounds as compared to m-PEG-SH (Fig. 3h).

CA and LA displayed a similar corona composition on Au NPs likely due to their negative charge caused by the carboxylic acid group and their small size (~200 Da). This favors the interaction with SRFA molecules *via* cation-bridging and also of SRFA directly with the Au surface due to

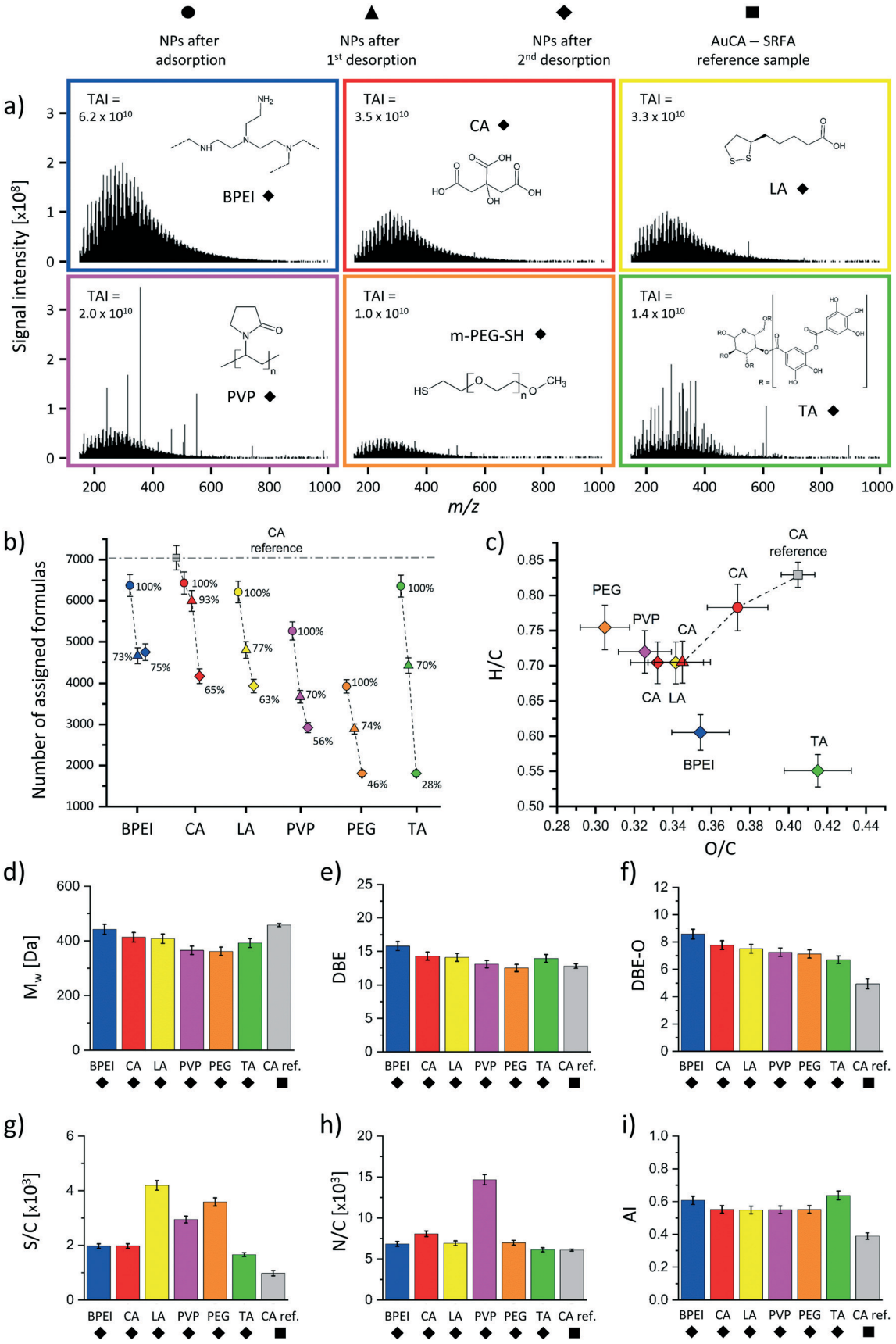

Fig. 3 Summary of the corona characteristics for all capping agents derived from LDI-FT-ICR-MS measurements. The LDI measurement error (4.2%) was calculated from triplicate sample preparation of the Au-CA – SRFA reference sample and was used for all LDI measurements. a) Shows reconstructed LDI-FT-ICR-MS spectra, b) number of assigned MFs, c) calculated molecular descriptors H/C *vs.* O/C plotted in an aVKD, and additional calculated molecular descriptors in d) M_w, e) DBE, f) DBE-O, g) S/C, h) N/C, and i) AI as bar plots.

a low steric hindrance. The chemical composition of their coronas was thus, highly similar based on the obtained H/C and O/C ratios, as well as M_w, DBE, DBE-O, and AI (Fig. 3c–f and i). Yet, LDI-FT-ICR-MS revealed small differences in the corona composition, indicating that Au-LA corona had a substantially higher S/C ratio as compared to Au-CA (Fig. 3g).

In contrast, the amine groups of Au-BPEI are positively charged and – despite its large molecular size – supported the attraction of SRFA molecules leading to the most extensive corona formation (Fig. 3a and b). This corona on BPEI appeared to be very strongly bound since the 2nd desorption step did not lead to any additional desorption (Fig. 3b). Moreover, Au-BPEI showed preferential interaction with large, oxygen-rich, and highly aromatic molecules shown by the highest M_w, DBE, DBE-O, high AI, O/C, and low H/C (Fig. 3c–f and i).

A notable exception from the observed trend was the corona of Au-TA which consisted of highly oxygen-rich aromatic molecules (highest O/C, AI and lowest H/C, DBE-O) as well as the lowest S/C and N/C ratios (Fig. 3c and f–i). The phenol moieties of TA may explain this adsorption behavior because they specifically interacted with similar molecular structures in SRFA. This is further supported by the slightly higher O/C ratio compared to the Au-CA – SRFA reference sample (Fig. 3c). Polyphenols are abundant in SRFA and tend to self-associate and form aggregates in aqueous solution through π–π stacking.[47] This may explain the specific adsorption pattern of SRFA on Au-TA and again emphasizes the substantial influence of the capping agent chemistry on the NP corona formation.

Overall, the capping agents are determining the extent and character of the corona formation. In order to accurately and directly characterize the coronas formed on different NP cores or capping agents, to study their stability, and explain their physicochemical behavior, a case-by-case study is required. Here, LDI-FT-ICR-MS is a promising method that is suggested to be used complementarily to other surface-sensitive analytical techniques to characterize NP–NOM interactions in future studies.

Conclusions

In this study, LDI-FT-ICR-MS was introduced as a method for the direct characterization of the NPs' corona after interaction of NPs with NOM. The method was validated by comparison of Au-CA NPs after multiple washing steps and complementary analysis by the indirect approach using ESI-FT-ICR-MS. The comparison revealed that although both techniques selectively ionize molecules from NOM, they can be used in a complementary way to validate each other. Nevertheless, if a comprehensive molecular composition picture of the sorption–desorption equilibrium and changes thereof is of interest, then both techniques should be used complementarily. Here LDI, in contrast to ESI, proved its applicability at high NOM : NP ratios and may easily be used in future to study natural systems without the need to extract the supernatant/dissolved phase. In the second step, LDI-FT-ICR-MS was applied to investigate the selective adsorption of SRFA based on five additional capped Au NPs varying in capping agent characteristics. Our results showed that i) LDI can identify variations in corona formation and ii) the corona extent and its molecular composition depend on the functional groups and the surface charge of the capping agents. This indicates that a case-by-case study is necessary to accurately describe the corona formation. Overall the capping agent appears as a key factor in determining the scale and type of interactions that a specific NP (core) will have with the environment. Only when fully considering the contribution of capping agents, a complete understanding of the corona formation and hence, a correct prediction of the environmental fate after exposure can be obtained. For instance, favorable or not favorable NOM adsorption will influence colloidal stability or aggregation determining uptake, transport, toxicity, and bioaccumulation of NPs in organisms. Finally, we propose for future NP–NOM interaction studies to additionally implement the use of LDI-FT-ICR-MS as an alternative direct characterization method to elucidate the full interactions at the bio–nano interface.

Conflicts of interest

There are no conflicts of interest to declare.

Acknowledgements

The funding of the project Analytical and Characterisation Excellence (ACEnano) within the European Union Horizon 2020 Program (H2020, grant agreement number 720952) is gratefully acknowledged. The authors appreciate the support of the ProVIS Centre for Chemical Microscopy at the Helmholtz Centre for Environmental Research – UFZ which is funded by the European Regional Development Funds (EFRE - Europe funds Saxony), the federal state of Saxony (Freistaat Sachsen), and the Helmholtz Association. We thank Jan Kaesler for the LDI- and ESI-FT-ICR-MS measurements and Kai Franze for software development. Finally, we thank Martin Lohse and Maria K. Ullrich for fruitful discussions and suggestions (all UFZ). The authors also thank the editor, Zhang Lin, and the anonymous reviewers for their constructive comments.

Notes and references

1 R. Grillo, A. H. Rosa and L. F. Fraceto, *Chemosphere*, 2015, **119**, 608–619.
2 M. Markiewicz, J. Kumirska, I. Lynch, M. Matzke, J. Köser, S. Bemowsky, D. Docter, R. Stauber, D. Westmeier and S. Stolte, *Green Chem.*, 2018, **20**, 4133–4168.
3 G. V. Lowry, K. B. Gregory, S. C. Apte and J. R. Lead, *Environ. Sci. Technol.*, 2012, **46**, 6893–6899.
4 S. M. Louie, R. D. Tilton and G. V. Lowry, *Environ. Sci.: Nano*, 2016, **3**, 283–310.

5 Z. Wang, L. Zhang, J. Zhao and B. Xing, *Environ. Sci.: Nano*, 2016, **3**, 240–255.
6 M. C. Surette and J. A. Nason, *Environ. Sci.: Nano*, 2016, **3**, 1144–1152.
7 M. C. Surette and J. A. Nason, *Environ. Sci.: Nano*, 2019, **6**, 540–553.
8 M. Kühn, N. P. Ivleva, S. Klitzke, R. Niessner and T. Baumann, *Sci. Total Environ.*, 2015, **535**, 122–130.
9 Z. Tang, X. Zhao, T. Zhao, H. Wang, P. Wang, F. Wu and J. P. Giesy, *Environ. Sci. Technol.*, 2016, **50**, 8640–8648.
10 V. L. Pallem, H. A. Stretz and M. J. M. Wells, *Environ. Sci. Technol.*, 2009, **43**, 7531–7535.
11 H. Wei, W. Leng, J. Song, C. Liu, M. R. Willner, Q. Huang, W. Zhou and P. J. Vikesland, *Environ. Sci. Technol.*, 2019, **53**, 575–585.
12 S. M. Louie, R. D. Tilton and G. V. Lowry, *Environ. Sci. Technol.*, 2013, **47**, 4245–4254.
13 S. M. Louie, E. R. Spielman-Sun, M. J. Small, R. D. Tilton and G. V. Lowry, *Environ. Sci. Technol.*, 2015, **49**, 2188–2198.
14 B. P. Koch, M. Witt, R. Engbrodt, T. Dittmar and G. Kattner, *Geochim. Cosmochim. Acta*, 2005, **69**, 3299–3308.
15 T. Reemtsma, *J. Chromatogr. A*, 2009, **1216**, 3687–3701.
16 J. Lv, S. Zhang, S. Wang, L. Luo, D. Cao and P. Christie, *Environ. Sci. Technol.*, 2016, **50**, 2328–2336.
17 S. Avneri-Katz, R. B. Young, A. M. McKenna, H. Chen, Y. E. Corilo, T. Polubesova, T. Borch and B. Chefetz, *Org. Geochem.*, 2017, **103**, 113–124.
18 T. Ohno, R. L. Sleighter and P. G. Hatcher, *Geoderma*, 2018, **326**, 156–163.
19 E. K. Coward, T. Ohno and A. F. Plante, *Environ. Sci. Technol.*, 2018, **52**, 1036–1044.
20 E. K. Coward, T. Ohno and D. L. Sparks, *Environ. Sci. Technol.*, 2019, **53**, 642–650.
21 Y. Wang, Z. Zhang, L. Han, K. Sun, J. Jin, Y. Yang, Y. Yang, Z. Hao, J. Liu and B. Xing, *Chem. Geol.*, 2019, **520**, 69–76.
22 T. D. Sowers, K. L. Holden, E. K. Coward and D. L. Sparks, *Environ. Sci. Technol.*, 2019, **53**, 4295–4304.
23 Y. Ding, Y. Lu, P. Liao, S. Peng, Y. Liang, Z. Lin, Z. Dang and Z. Shi, *Environ. Sci.: Nano*, 2019, **6**, 2037–2048.
24 M. Baalousha, K. Afshinnia and L. Guo, *Environ. Sci.: Nano*, 2018, **5**, 868–881.
25 C. S. Ho, C. W. K. Lam, M. H. M. Chan, R. C. K. Cheung, L. K. Law, L. C. W. Lit, K. F. Ng, M. W. M. Suen and H. L. Tai, *Clin. Biochem. Rev.*, 2003, **24**, 3–12.
26 Z. J. Zhu, V. M. Rotello and R. W. Vachet, *Analyst*, 2009, **134**, 2183–2188.
27 K. Giannopoulos, O. J. Lechtenfeld, T. R. Holbrook, T. Reemtsma and S. Wagner, *Anal. Bioanal. Chem.*, 2020, **412**, 5261–5271.
28 M. Das, K. H. Shim, S. S. A. An and D. K. Yi, *J. Toxicol. Environ. Health Sci.*, 2011, **3**, 193–205.
29 O. J. Lechtenfeld, G. Kattner, R. Flerus, S. L. McCallister, P. Schmitt-Kopplin and B. P. Koch, *Geochim. Cosmochim. Acta*, 2014, **126**, 321–337.
30 T. Kind and O. Fiehn, *BMC Bioinf.*, 2007, **8**, 105.
31 B. P. Koch, G. Kattner, M. Witt and U. Passow, *Biogeosciences*, 2014, **11**, 4173–4190.
32 P. Herzsprung, N. Hertkorn, W. von Tümpling, M. Harir, K. Friese and P. Schmitt-Kopplin, *Anal. Bioanal. Chem.*, 2014, **406**, 7977–7987.
33 B. P. Koch and T. Dittmar, *Rapid Commun. Mass Spectrom.*, 2006, **20**, 926–932.
34 S. Kim, R. W. Kramer and P. G. Hatcher, *Anal. Chem.*, 2003, **75**, 5336–5344.
35 N. Tayyebi Sabet Khomami, A. Philippe, A. A. Abu Quba, O. J. Lechtenfeld, J.-M. Guigner, S. Heissler and G. E. Schaumann, *Environ. Sci.: Nano*, 2020, **7**, 486–500.
36 A. Bauzá and A. Frontera, *Inorganics*, 2018, **6**, 64.
37 A. Frontera and A. Bauzá, *Chem. – Eur. J.*, 2018, **24**, 7228–7234.
38 M. de las N. Piña, A. Frontera and A. Bauzá, *J. Phys. Chem. Lett.*, 2020, **11**, 8259–8263.
39 T. Bürgi, *Nanoscale*, 2015, **7**, 15553–15567.
40 R. C. Hoft, M. J. Ford, A. M. McDonagh and M. B. Cortie, *J. Phys. Chem. C*, 2007, **111**, 13886–13891.
41 M. J. Ford, R. C. Hoft and J. D. Gale, *Mol. Simul.*, 2006, **32**, 1219–1225.
42 S. Diegoli, A. L. Manciulea, S. Begum, I. P. Jones, J. R. Lead and J. A. Preece, *Sci. Total Environ.*, 2008, **402**, 51–61.
43 J. Liu, S. Legros, G. Ma, J. G. C. Veinot, F. von der Kammer and T. Hofmann, *Chemosphere*, 2012, **87**, 918–924.
44 C. E. McNamee, S. Yamamoto and K. Higashitani, *Biophys. J.*, 2007, **93**, 324–334.
45 K. M. Koczkur, S. Mourdikoudis, L. Polavarapu and S. E. Skrabalak, *Dalton Trans.*, 2015, **44**, 17883–17905.
46 H. Wen, K. R. Morris and K. Park, *J. Pharm. Sci.*, 2005, **94**, 2166–2174.
47 V. de Freitas, in *Recent Advances in Polyphenol Research*, John Wiley & Sons, Ltd, Chichester, UK, 2019, pp. 263–284.

